Multiple Sclerosis and Related Disorders 15 (2017) 27–33

Contents lists available at ScienceDirect

Multiple Sclerosis and Related Disorders

journal homepage: www.elsevier.com/locate/msard

Reduction of PK11195 uptake observed in multiple sclerosis lesions after natalizumab initiation

Ulrike W. Kaunzner[a,1], Yeona Kang[b,1], Elizabeth Monohan[a], Paresh J. Kothari[b], Nancy Nealon[a], Jai Perumal[a], Timothy Vartanian[a], Amy Kuceyeski[c], Shankar Vallabhajosula[b], P. David Mozley[b], Claire S. Riley[d], Stephen M. Newman[e], Susan A. Gauthier[a,*]

[a] Judith Jaffe Multiple Sclerosis Center, Weill Cornell Medicine, 1305 York Avenue, New York City, NY, USA
[b] Department of Radiology/Nuclear Medicine, Weill Cornell Medicine, New York, 516 E 72nd St, New York City, NY, USA
[c] Brain and Mind Research Institute, 407 East 61st street, New York City, NY, USA
[d] Multiple Sclerosis Clinical Care and Research Center, Columbia University, 710 West 168th street, New York City, NY, USA
[e] Island Neurological, 824 Old Country Road #1, Plainview, NY, USA

ARTICLE INFO

Keywords:
Multiple sclerosis
Natalizumab
Microglia/Macrophages
PK11195-PET
Lesion

ABSTRACT

Objective: The objective of this study is to longitudinally analyze the uptake of [^{11}C]PK11195-PET in multiple sclerosis patients after 3 and 6 months of natalizumab treatment.
Methods: Eighteen MS patients, starting treatment with monoclonal anti-VLA-4, were enrolled in a longitudinal PK-PET study. PK uptake was quantified by volume of distribution (VT) calculation using image-derived input function at baseline, 3 and 6 months. Pharmacokinetic quantification was done using a segmented MRI, and selected areas included white matter, gadolinium enhancing lesions, non-enhancing lesions, cortical grey matter and thalamus. VTs of lesions were calculated in reference to each patient's white matter (VT ratio = VTr), to consider physiologic variability.
Results: Test–retest variability was stable for healthy control (HC). Quantification of PK uptake was completed in 18 patients, and baseline uptake was compared to 6-month uptake. After the start of natalizumab VTr significantly decreased in 13 individual enhancing lesions present within 5 patients ($p = 0.001$). Moreover, VTr of the sum of non-enhancing lesions showed a moderate decrease ($p = 0.03$). No longitudinal changes were detected in normal appearing white matter, the thalamus and cortical grey matter.
Conclusion: A reduction in PK11195 uptake was observed in both enhancing and chronic lesions after the start of natalizumab. PK11195 PET can be used as tool to assess the longitudinal change in MS lesions.

1. Introduction

PET imaging in combination with the ligand [^{11}C]PK11195 (PK) can be used to evaluate activated microglia and macrophages (MG/MΦ) in vivo (Banati, 2002). PK binds to the translocator protein (TSPO), which is expressed on the outer mitochondria membrane of activated MG/MΦ (Banati et al., 2000; Jucaite et al., 2012). Studies with PK confirmed the most prominent uptake within areas of increased inflammation, especially in enhancing lesions in multiple sclerosis (MS) patients (Debruyne et al., 2003), however most studies evaluating the binding of TSPO have been cross-sectional in design.

The innate immune system plays a pivotal role in the pathophysiology of MS, and important cell types involved in this process are resident microglia and blood-derived macrophages (Gandhi et al., 2010). In acute MS lesions, activated MG/MΦ are involved in demyelination and are the source of reactive nitrogen and oxygen species, which induces oxidative injury to mitochondria, oligodendrocytes and degenerating neurons (Fischer et al., 2012). Iron-containing pro-inflammatory MG/MΦ are present at the rim of chronic active MS lesions and at the site of ongoing demyelination (Mehta et al., 2013).

Natalizumab is a monoclonal antibody (AB) directed against VLA-4, an alpha-4 integrin expressed on leukocyte surfaces (Yednock et al., 1992). This protein interacts with its ligand, vascular cell adhesion molecule 1 (VCAM-1), which is located on endothelium, as well as on MG/MΦ and astrocytes (Chabot et al., 1997; Peterson et al., 2002). Blocking the VLA-4/VCAM-1 interaction decreases the influx of lymphocytes, reducing the effects of the adaptive immune response in the CNS, and subsequently the activation of microglia (del Pilar Martin

* Corresponding author.
E-mail address: sag2015@med.cornell.edu (S.A. Gauthier).
[1] Same contributing author.

http://dx.doi.org/10.1016/j.msard.2017.04.008
Received 21 October 2016; Received in revised form 20 April 2017; Accepted 20 April 2017
2211-0348/ © 2017 Elsevier B.V. All rights reserved.

et al., 2008; Waisman et al., 2015). In human studies, natalizumab therapy was shown to be highly effective for relapsing remitting MS (RRMS) with a significant reduction in relapse rates and MRI lesion activity (Miller et al., 2003; Johnson, 2007).

The current study aims to use PK11195-PET to evaluate the longitudinal uptake of PK11195 in a cohort of MS patients following the initiation of natalizumab treatment.

2. Methods

2.1. Human participants

This longitudinal study analyzed the degree of PK11195 uptake in natalizumab treated MS patients. The medication effect on PK11195 uptake was assessed over the period of 6 months (mo), using PK-PET imaging. Twenty-four patients with the diagnosis of RRMS or secondary progressive MS (SPMS) were enrolled in the study. However, the PET data from two participants had to be discarded because they were confounded by excessive motion, and four patients decided to withdraw consent. The eighteen remaining patients were used for the analysis. This study was approved by an ethical standards committee on human experimentation, and written informed consent was obtained from all patients. Patient characteristics and clinical data were obtained within 1mo of the individual's brain MRI and PK-PET scan (Supplementary Table 1). The following clinical data were collected: gender, age, disease duration (DD), Expanded Disability Status Score (EDSS), disease subtype, disease modifying therapy (DMT), duration of washout of prior medication, amount of enhancing lesions (EL) immediately prior to natalizumab start and time of steroids and natalizumab in reference to the individual imaging modalities. Patients were followed with MRI and PK-PET scans at baseline, 3mo and 6mo post natalizumab treatment.

Five healthy controls (HC) were recruited for test and retest PK-PET scans to confirm the repeatability of the PK quantification method. Institutional review board approval was obtained.

2.2. MRI data acquisition and processing

2.2.1. MRI acquisition

A 3Tesla GE scanner (Hdxt 16.0) with an 8-channel phased-array coil was used and T1-weighted sagittal 3D-BRAVO ($1.2\times1.2\times1.2$ mm) with and without gadolinium enhancement, T2 ($0.5\times0.5\times3$ mm), T2-FLAIR ($1.2\times0.6\times0.6$ mm) sequences were obtained. MRI scans were obtained within 4 weeks of the PET scans.

2.2.2. MRI Tissue and lesion segmentation

White matter (WM) segmentation with FreeSurfer (Dale et al., 1999; Fischl et al., 1999a, 1999b) and a semi-automated lesion mapping method was used on the acquired T1 and T2 data. First, the WM and grey matter (GM) masks were segmented from the T1 images and were checked and edited for misclassification due to WM T1-hypointensities associated with lesions (Chard et al., 2010). The WM hyperintensity lesion masks were created from the T2 FLAIR images by categorizing the tissue type based on the image intensities. They were then masked with the segmented FreeSurfer WM volume to include only WM abnormalities. All the images were aligned onto FreeSurfer volume with the boundary-based registration. The WM lesion masks were overlaid on T2 and T2 FLAIR images and a trained neurologist (SG) gave a final approval on edits.

We identified EL among the cohort. Separate regions of interests (ROI) were created for these lesions, which were analyzed as individual EL. A secondary non-enhancing lesion (NEL) mask was created by subtracting the specific enhancing lesion ROI from the previous created WM lesion mask.

2.3. PK radioligand production and PET imaging

The radioligand [N-methyl-11C](R)-1-(2-chlorophenyl)-N-(1-methylpropyl) − 3-isoquinolinecarboxamide, known as [^{11}C]PK11195 was prepared by modifying previously described procedures (Zhang et al., 2001). Briefly, 1 mg (2.95 μmol) desmethyl- PK11195 in 350 μl DMSO was treated with 10 μmol aqueous sodium hydroxide and allowed to react with (C-11) methyliodide. Following reaction [^{11}C] PK11195 was purified by high pressure liquid chromatography (HPLC) and formulated in saline with 7% ethanol.

Following intravenous administration of 370–555 MBq (10–15 mCi) of [^{11}C]PK11195, dynamic PET scans over a period of 60 min were acquired in list mode with the same whole body PET/CT scanner (mCT, Siemens/CTI, Knoxville, TN). In HC and MS participants, test-retest scans were obtained on the same day with an approximate time interval of about 2 h.

The PET camera has a spatial resolution of ~4 mm measured as the reconstructed full-width at half maximum of a point source in air. PET scans were corrected for photon absorption and scatter, using an in-line CT scanner set at 120 kV, a pitch of 1.5, and 30 mA. PET data were reconstructed in a 400×400 matrix with a voxel size of $1.082\times1.082\times2.025$ mm^3 using a zoom of 2.0 and an iterative + time of flight (TOF) list-mode reconstruction algorithm provided by the manufacturer.

2.4. PET data analysis

Images were reconstructed into 22 frames (4 frames of 15 s each, then 4×30 s, 3×60 s, 2×120 s, 8×300 s and 1×600 s). For the image-derived input function (IDIF), circular ROI measuring 4 mm in diameter were placed manually in the C4 area of the carotid artery on summed transaxial PET images acquired between 90-to-120 s after the start of the 60 s infusion. These ROIs were then automatically transposed onto the other frames without further operator input.

Summed PET images were co-registered to their corresponding MRI scans using PMOD® (PMOD Technologies Ltd., Zurich Switzerland) (Mikolajczyk et al., 1998). ROIs were co-registered with the PET images to interrogate the normal appearing white matter (NAWM), cortical grey matter (CGM), thalamus (TH), total NEL and individual EL.

2.5. PET quantification

To determine the most appropriate quantification approach, we compared a blood based direct method (IDIF) with an indirect method based upon brain tissue reference region (SuperPK (Turkheimer et al., 2007)).

2.5.1. IDIF

For the estimation of PK volume of distribution (VT) the concentration of radioactivity in brain and whole blood was applied to the Logan graphical method (Logan et al., 1990). Population metabolite data were used to correct to the input function (Roivainen et al., 2009). Image and kinetic analyses were performed using PMOD 3.4. VT ratio (VTr), which was defined as a ratio of VT within a specific ROI divided by the VT value of an individual's NAWM was also analyzed. VTr was calculated to control for normal physiological variability, which is known to influence absolute VT measurements (Hammoud et al., 2005). NAWM had a stable PK uptake over time (baseline to 6mo, $p=0.79$), and was considered as ideal reference tissue to calculate the ratio. VT and VTr results were compared for the subsequent ROI analysis.

2.5.2. SuperPK

PET Quantification was also calculated using the Logan reference tissue model that uses a reference tissue input function. The tissue reference input was extracted from the PK-PET dynamic data using SuperPK software.

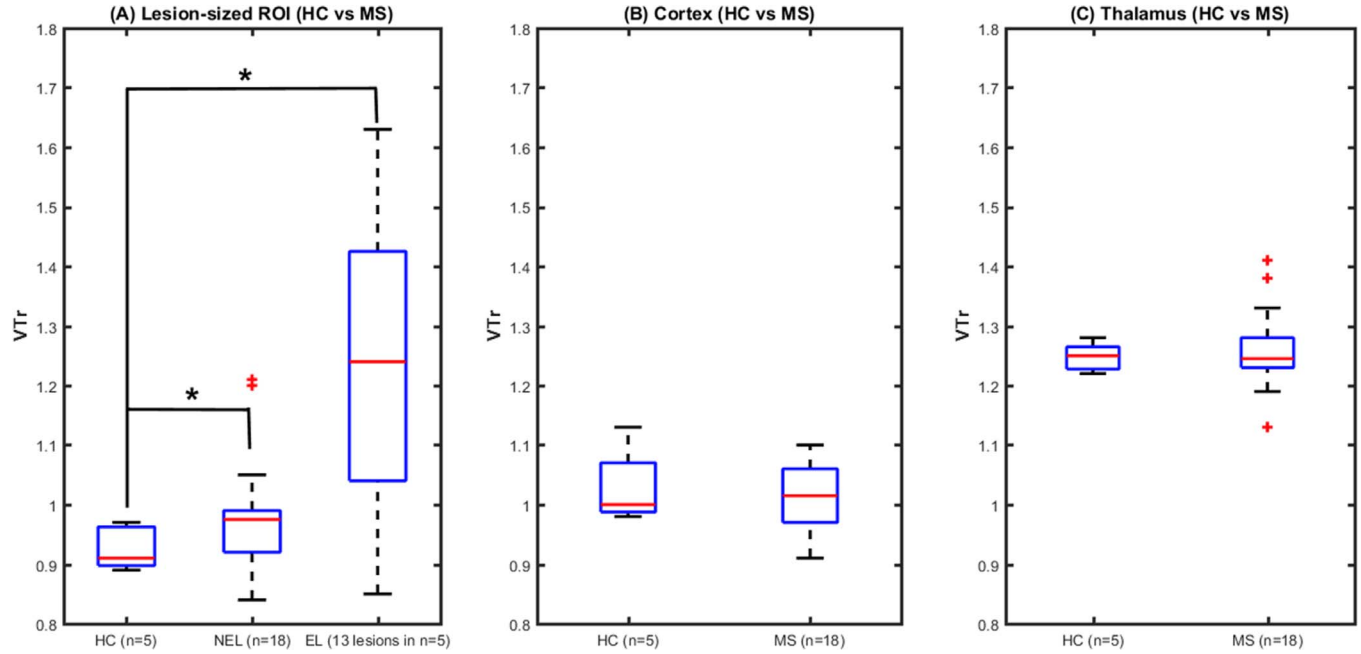

Fig. 1. Detection of PK within MS lesion subtypes. VTr within HC lesion-sized ROI, NEL and EL was calculated as an average within the full lesion mask per participant as opposed to individual lesions. VTr was higher in NEL ($p = 0.05$) and EL ($p = 0.03$) compared to HC lesion-sized ROI (Fig. 1A). VTr was similar between HC and MS patients within CGM ($p = 0.51$, Fig. 1B) and the TH ($p = 0.69$, Fig. 1C).

2.6. Test-retest variability

Grey matter and lesion based PK variability assessment was performed in five HC participants. HC T1W images were automatically processed using the FreeSurfer's cross sectional stream. Eq. (1) calculated variability of the test-retest scans for WM, CGM, TH and NAWM for the two PET quantification approaches. Supplementary Table 2 compares IDIF and SuperPK data in HC, and revealed that IDIF provided more consistent variability in reproducibility testing, indicating a more reliable result. In addition, VTr showed much less variability as compared to VT, confirming the stability of this measure. Therefore, IDIF and VTr were considered most appropriate to represent change in our analysis.

2.6.1. Lesion-sized variability

To appropriately represent a change beyond IDIF variability within NEL masks and individual EL, we created a representative lesion-sized ROI for HC. The HC lesion-sized ROI was created from a combination of ten randomly created WM lesion ROIs. The volume of HC lesion-sized ROI was $5.3 \pm 1.2[c^3m]$ and fell between the volumes of NEL ($19.8 \pm 23.0[c^3m]$) and EL ($4.9 \pm 7.4[c^3m]$). Test-retest variability was calculated (Eq. (1)) for the HC lesion-sized ROI and will be used as the reference for the longitudinal patient analysis.

2.7. Statistical analyses

2.7.1. PET analysis

The variability of longitudinal measurements within participants was analyzed by means of descriptive statistics: mean, SD, coefficient of variance (CV), and absolute variability (Eq. (1)):

$$\text{Var}(\%) = 100*\text{abs}(\text{VTr (baseline)} - \text{VTr (3mo/6mo)}) / (0.5*(\text{VTr (baseline)} + \text{VTr (3mo/6mo)})) \quad (1)$$

The descriptive statistics and computations for longitudinal analysis of the absolute VTr values were performed using SPSS (IBM Corp. Version 22.0. Armonk, NY: IBM Corp). In all analyses, the statistical significance (alpha level) was set at $p < 0.05$, using the non-parametric Wilcoxon rank sum test.

2.7.2. Analysis of covariance (ANCOVA)

ANCOVA was used to estimate mean change in VTr within NEL from baseline to 6mo among patients with EL compared to patients without EL, controlling for the independent effects of age of patient, steroid use and VTr at baseline. A separate ANCOVA model was used to estimate mean VTr change, controlling for the independent effects of disease duration and VTr at baseline.

3. Results

3.1. MS Patient cohort

This was a longitudinal, prospective study of PK11195 uptake in patients initiating natalizumab therapy. Patients were followed with MRI and PK-PET scans at baseline, 3mo and 6mo post natalizumab treatment. The eighteen patients utilized for this analysis are described in detail in Supplementary Table 1. Thirteen women and five men completed the study and mean age was 37.3 years. Mean disease duration, before starting natalizumab, was 8.2 years. The majority of patients were switching therapy to natalizumab; however, 5 patients were treatment naïve. Reason for switching to natalizumab was treatment failure of other disease modifying agents, or active disease with high lesion burden in the patients who were started on natalizumab. Out of the 18 patients, 13 patients underwent PET scans at 3mo and 6mo, while all 18 patients received PET imaging at baseline and 6mo. The reasons for missed 3mo scans were scheduling conflicts on the patients' side. Of the 18 patients, 5 patients had EL on the initial MRI (36%), and out of these 5 patients one missed the 3mo PET scan. Five patients had received intravenous steroids within the 4 weeks prior to PET scan. The baseline EDSS was ranging between 0 and 6, and did not show a significant change over the course of 6mo.

3.2. PK detection within MS lesion subtypes

VTr within EL (1.23 ± 0.24) and NEL (0.98 ± 0.09) demonstrated a higher PK uptake as compared to HC lesion-sized ROI (0.93 ± 0.04), however only EL reached significance ($p = 0.03$ vs. $p = 0.05$), Fig. 1A. The VTr for HC CGM (1.03 ± 0.06) was similar to that of MS patients

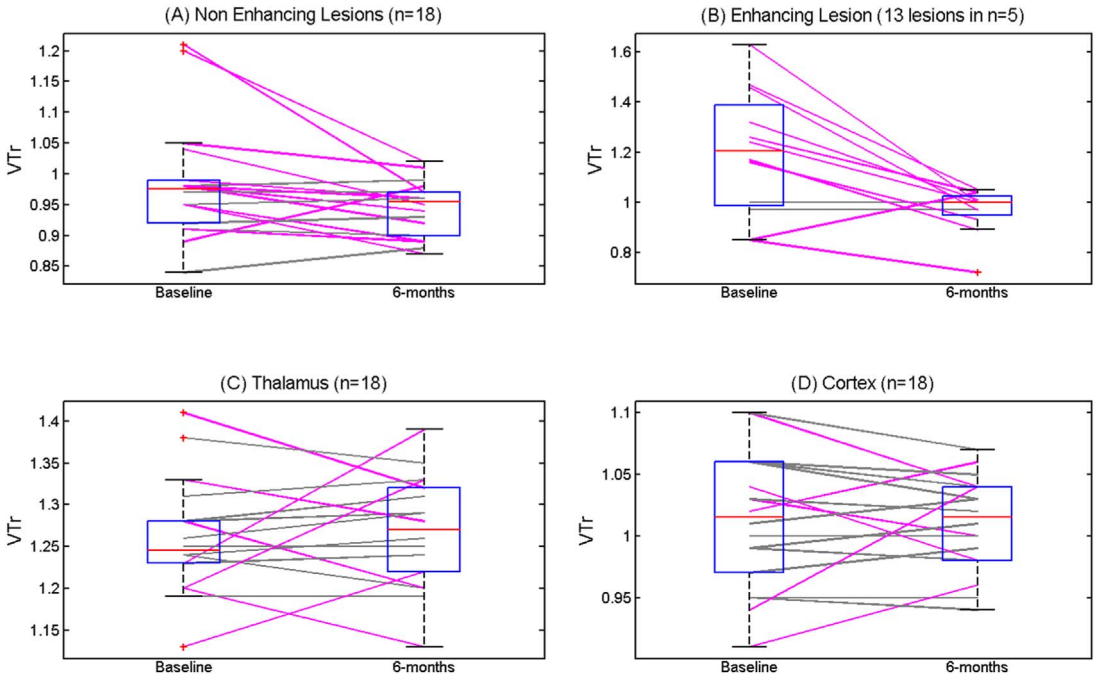

Fig. 2. Regional changes in PK uptake after treatment with natalizumab. VTr within NEL was calculated as the average within the full lesion mask per patient; VTr within EL was calculated for individual lesions. VTr significantly decreased over the course of 6mo within NEL ($p = 0.03$, Fig. 2A), and EL ($p = 0.001$, Fig. 2B). No significant change was detected within the TH ($p = 0.86$, Fig. 2C) or CGM ($p = 0.58$, Fig. 2D). Magenta color visualizes the change in VTr that is above the noise established with HC.

(1.01 ± 0.05), $p = 0.51$, Fig. 1B. VTr was also not significantly different for the TH, comparing HC (1.25 ± 0.02) with MS patients (1.26 ± 0.07), $p = 0.69$, Fig. 1C.

3.3. PK uptake decreases in both non-enhancing and enhancing lesions after 6mo of natalizumab

3.3.1. IDIF HC lesion-sized ROI variability

Five HC underwent test-retest PK-PET imaging to determine the variability of PK IDIF in HC lesion-sized ROI. No significant difference in the VTr was observed for the selected test-retest HC ROI (Variability 2.93%, $p = 0.24$).

3.3.2. Longitudinal patient analysis

All 18 patients underwent PET imaging at baseline and 6mo. The VTr of NEL (mean NEL volume for 18 subjects: 12.44 ± 13.60 cm^3) decreased from 0.98 to 0.94 ($p = 0.03$) (Fig. 2A). Fig. 2A demonstrates that the change in the sum of NEL exceeded the calculated lesion-sized IDIF variability, suggesting true biological change. Five patients (36%) presented initially with a total of 13 individual EL (mean EL volume for individual lesions ($n = 13$ lesions): 4.88 ± 7.41 cm^3). The VTr of individual EL showed a significant decrease from 1.23 ± 0.22 to 0.97 ± 0.009 at 6mo ($p = 0.001$, Fig. 2B).

To further ensure the change in PK in NEL within patients having EL was not contaminated by immune activity of adjacent EL, we utilized an ANCOVA analysis to compare the two groups controlling for various clinical characteristics. There was no difference in change of VTr within NEL between the two patient populations ($p = 0.63$) after controlling for age of patient, steroid use and VTr at baseline. Importantly, steroid use prior to natalizumab treatment was not associated with change in VTr of NEL ($p = 0.69$). An ANCOVA controlling for the independent effect of DD and VTr at baseline revealed a similar change in VTr within NEL between the two groups ($p = 0.51$).

TH and CGM did not reveal a change in VTr over the course of 6mo. Interestingly, some patients demonstrated an upward or downward trend in VTr that exceeded the variance in repeated studies of HC; however, the CGM changes were not consistent among individual patients (Fig. 2C and D).

VT and VTr results for the longitudinal analysis of EL, NEL, TH and CGM were compared. Both VT and VTr changed for EL, while NEL showed significant decrease when using VTr but no significance, when VT was used (Table 1).

3.4. Time course of PK uptake in enhancing lesions

The time course for reduction of PK11195within individual EL, after initiation of natalizumab, was further evaluated in the 4 patients who had 3 and 6mo PET scans. These four patients had a total of 12 EL. The VTr of the 12 EL lesions decreased from 1.23 to 1.0 within the first 3mo ($p < 0.003$) and plateaued after another 3mo (0.96 ± 0.09, $p = 0.096$) (Fig. 3). None of the 12 EL had gadolinium enhancement at 3 and 6mo after initiating treatment. The decline in PET signal can be visualized in

Table 1
Comparison of VT and VTr.

VT (n = 18)	baseline	6month	p-value	VTr (n = 18)	baseline	6month	p-value
NEL	0.88 ± 0.26	0.83 ± 0.17	0.33	NEL (18)	0.98 ± 0.09	0.94 ± 0.04	0.03
NAWM	0.89 ± 0.24	0.88 ± 0.17	0.96	NAWM	1	1	
GM	0.90 ± 0.23	0.89 ± 0.17	0.98	GM	1.01 ± 0.05	1.01 ± 0.04	0.58
TH	1.13 ± 0.31	1.12 ± 0.24	0.96	TH	1.26 ± 0.06	1.27 ± 0.07	0.86
EL(13 in n = 5)	1.12 ± 0.19	0.85 ± 0.13	0.008	EL(13 in n = 5)	1.23 ± 0.23	0.97 ± 0.09	0.001

VT and VTr results for NEL, NAWM, GM, TH and EL are visualized at baseline and after 6mo of natalizumab treatment. Results are shown for 18 patients for NEL, NAWM, GM and TH. Results are shown for 13 EL in 5 patients. NEL = non-enhancing lesion, NAWM = normal appearing white matter, GM = grey matter, TH = Thalamus, EL = enhancing lesion.

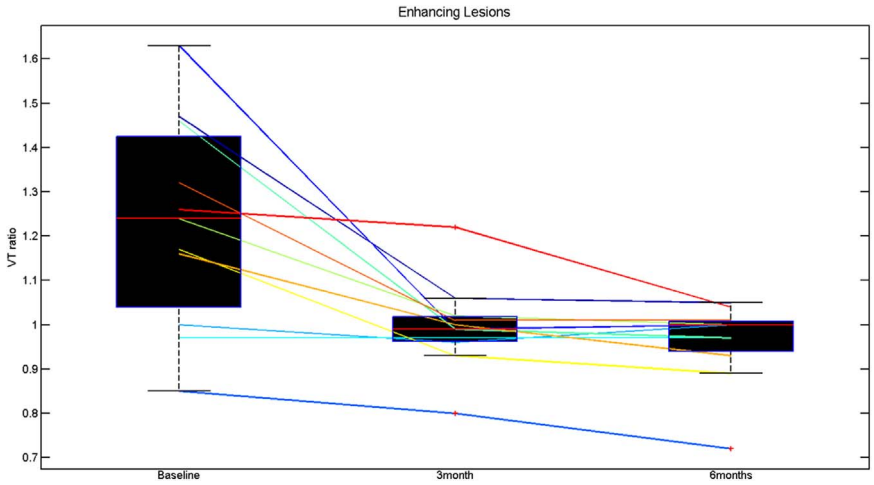

Fig. 3. Change in PK uptake within individual enhancing lesions. The time course of the change in VTr of PK11195 within 12 individual enhancing lesions after treatment with natalizumab is represented. PK uptake decreased from baseline to 3mo ($p = 0.003$) and remained stable between 3mo and 6mo ($p = 0.096$).

the parametric image of a typical lesion (Supplementary Fig. 1).

4. Discussion

We have shown a reduction in PK11195 uptake in MS patients following treatment with anti-VLA4 (natalizumab). We identify a longitudinal decrease of PK11195 uptake in EL, which was anticipated, however we also observe a decrease in this ligand's uptake in NEL. This study supports the potential utilization of PK-PET as an in vivo tool to assess the longitudinal effects of disease modifying agents in MS patients.

PK-PET imaging is a well-established method to assess CNS inflammation, and has been used to investigate activated MG/MΦ in the cortex of MS patients (Politis et al., 2012), as well as in NAWM of patients with clinically isolated syndrome (Giannetti et al., 2015). These studies described cross sectional PK binding in MS patients as compared to HC, and so far, only two longitudinal analyses of TSPO binding following treatment initiation have been reported. One study investigated the longitudinal effect of glatiramer acetate (Ratchford et al., 2012) and showed a significant decrease of PK11195 in GM and WM. Another recently published study analyzed the effect of fingolimod on MS lesions, which demonstrated a significant decrease in PK11195 signal for the combined T2 lesion area (Sucksdorff et al., 2017). Similarly, this study was unable to appreciate a longitudinal change in PK11195 in GM or NAWM. Comparing our results to these studies is difficult given the differences in PET quantification methods, patient cohort sizes and medications. However, the latter study supports our findings of longitudinal change of PK11195 signal in NEL and no significant change in GM and NAWM.

PK was the selected marker, since it is frequently used ligand for research purposes, with an affinity to activated MG/MΦ and established binding potential (Lockhart et al., 2003). PK, as a first generation TSPO ligand, has high non-specific binding as compared to the newer generation ligands, which presents a challenge to define a reference region. Multiple groups have explored various reference-region based quantification techniques and numerous compounds in attempt to improve accurate in vivo signal detection (Venneti et al., 2013). Importantly, there are still limitations to the newer generation of TSPO ligands such as genetic variability in binding affinity and conflicting results with in vivo studies, and it is unclear which are the best quantification methods for these agents (Boutin et al., 2015). In our hands HC test-retest data demonstrates stable repeatability as compared to SuperPK, and low variability is particularly important for the longitudinal assessment of PK11195 uptake. Moreover, SuperPK analysis generated low binding potential curves, and failed for a few subjects. Based on the comparisons of IDIF and SuperPK we feel that Logan-VT calculated with IDIF is the best representation of PK quantification. We have also separately studied patient test-retest variability in those on stable treatment (data not shown) which fell below our HC variability, therefore the decision was made to only utilize HC variability for this analysis. Lastly, given the known concentrated activity of MG/MΦ within active MS lesions, a lesion-to-NAWM Logan-VTr measurement for PK has been described as sufficiently informative despite its limitations (Chauveau et al., 2008). NAWM was chosen since lesions appear in this tissue compartment, and since NAWM VT showed stability in our longitudinal analysis. The level of inflammation within lesions and NAWM is expected to tend in the same direction and is thought not to influence the ratio. Importantly, VT and VTr demonstrated a similar result, however, as demonstrated in our table, VT has a much higher variability, which can explain the loss of significance in some of our results.

We found that the most prominent decrease in inflammation, following natalizumab treatment, occurred in active, gadolinium enhancing MS lesions. Analyzing this lesion type at two time points after the start of natalizumab showed that the most striking improvement occurred within the first 3mo. These results are consistent with a high level of innate immune activity occurring at the early lesion stage (Marik et al., 2007), however these findings must be interpreted with caution. Blood brain barrier (BBB) breakdown, represented by gadolinium enhancement, is a defining feature of acute lesions and can dramatically influence binding of TSPO radiotracers (Sridharan et al., 2017; Vowinckel et al., 1997). The situation is further complicated by the high non-specific binding associated with PK11195, thus the extent of activated MG/MΦ uptake reported may be over-estimated. However, histopathological studies have demonstrated that PK binding is significantly elevated in MS lesions secondary to binding of activated MG/MΦ (Banati et al., 2000; Vowinckel et al., 1997), which suggests that our results are, at least in part, related to the activity of these immune cells. Further studies are required to get an accurate assessment of the TSPO binding relative to changing BBB permeability. In addition, the observed reduction of PK in acute lesions may be solely related to the natural disease course, specifically the normal decline of inflammation known to occur after BBB closure (Rovira et al., 2013). A direct comparison with a control group would be ideal, however is difficult to conduct from a clinically and ethical point of view.

Chronic MS lesions are histologically divided into chronic active lesions with a gliotic center and a hypercellular rim, composed of activated MG/MΦ (Popescu et al., 2013), and chronic inactive lesions that lack the hypercellular rim of activated microglia. Our comparison of HC with MS patient PK11195 distribution demonstrated a trend

favoring a difference between HC WM and MS NEL. This suggests that PK11195 may represent the presence of activated MG/MΦ within a fraction of chronic lesions beyond the closure of the BBB. We measured a moderate decrease of PK11195 uptake in NEL, seen with VTr, which proposes that longitudinal changes in PK11195 can be appreciated in chronic lesions.

PK distribution within the cortex and TH was similar between HC and MS patient. This is in contrast to prior studies, showing increased cortical and thalamic binding of PK in MS patients, compared to HC (Politis et al., 2012). An explanation for this result disparity can be the different analysis: while their group used a reference-based quantification method and calculated PK binding potential, we analyzed our data based on the volume of distribution, since we saw more stability with this method for longitudinal analysis.

The small patient cohort and short time course are limitations to our study, however we plan to follow this cohort and obtain a PK-PET after 24mo of natalizumab treatment. Given the low number of participants, we combined patients with only NEL with patients also having EL. In the separate analysis we found similar trends, however we failed to reach a level of significance and feel that this result is likely due to the loss of statistical power associated with smaller sample sizes. In an attempt to further address the influence of EL, we included an ANCOVA analysis comparing the change in NEL among the two subgroups and revealed a similar change in NEL. Subsequent studies with larger samples can more comprehensively interrogate the potential influence of EL on PK uptake within NEL among individual patients. Other limitations include the time difference between PET scans and MRI, which might have influenced the results of the enhancing lesions.

We describe the longitudinal change of PK11195 uptake in MS patients, occurring after natalizumab treatment, utilizing IDIF quantification of PK-PET. Interestingly, not only PK11195 uptake in EL changed in response to treatment, but also NEL showed a decrease. This study demonstrates that PK-PET in combination with IDIF can serve as an in vivo tool to assess MS lesions over time, and can be used to monitor treatment responses.

Disclosures

Dr. Kaunzner received grant support from Biogen. Dr. Kang reports no disclosures. Ms. Monohan reports no disclosures. Dr. Kothari reports no disclosures. Dr. Nealon reports no disclosures. Dr. Perumal reports no disclosures. Dr. Vartanian is a speaker for Teva Neuroscience, has received honoraria for advising Genzyme, and has received grant support from the National MS society, Biogen, and Mallinckrodt. Dr. Kuceyeski reports no disclosures. Dr. Vallabhajosula reports no disclosures. Dr. Mozley has received grant support from Biogen. Dr. Riley reports no disclosures. Dr. Newman reports no disclosures. Dr. Gauthier has received grant support from Biogen, Novartis Pharmaceuticals, Mallinckrodt, and Genzyme.

Study funding

Supported by Biogen.

Acknowledgements

We acknowledge Gulce Askin, MPH and Linda Gerber, Ph.D. for their support with the statistical analysis.

Appendix A. Supporting information

Supplementary data associated with this article can be found in the online version at http://dx.doi.org/10.1016/j.msard.2017.04.008.

References

Banati, R.B., 2002. Visualising microglial activation in vivo. Glia 40, 206–217.
Banati, R.B., Newcombe, J., Gunn, R.N., et al., 2000. The peripheral benzodiazepine binding site in the brain in multiple sclerosis: quantitative in vivo imaging of microglia as a measure of disease activity. Brain 123 (Pt 11), 2321–2337.
Jucaite, A., Cselenyi, Z., Arvidsson, A., et al., 2012. Kinetic analysis and test-retest variability of the radioligand [11C](R)-PK11195 binding to TSPO in the human brain - a PET study in control subjects. EJNMMI Res. 2, 15.
Debruyne, J.C., Versijpt, J., Van Laere, K.J., et al., 2003. PET visualization of microglia in multiple sclerosis patients using [11C]PK11195. Eur. J. Neurol. 10, 257–264.
Gandhi, R., Laroni, A., Weiner, H.L., 2010. Role of the innate immune system in the pathogenesis of multiple sclerosis. J. Neuroimmunol. 221, 7–14.
Fischer, M.T., Sharma, R., Lim, J.L., et al., 2012. NADPH oxidase expression in active multiple sclerosis lesions in relation to oxidative tissue damage and mitochondrial injury. Brain: J. Neurol. 135, 886–899.
Mehta, V., Pei, W., Yang, G., et al., 2013. Iron is a sensitive biomarker for inflammation in multiple sclerosis lesions. PLoS One 8, e57573.
Yednock, T.A., Cannon, C., Fritz, L.C., Sanchez-Madrid, F., Steinman, L., Karin, N., 1992. Prevention of experimental autoimmune encephalomyelitis by antibodies against alpha 4 beta 1 integrin. Nature 356, 63–66.
Chabot, S., Williams, G., Yong, V.W., 1997. Microglial production of TNF-alpha is induced by activated T lymphocytes. Involvement of VLA-4 and inhibition by interferonbeta-1b. J. Clin. Investig. 100, 604–612.
Peterson, J.W., Bo, L., Mork, S., Chang, A., Ransohoff, R.M., Trapp, B.D., 2002. VCAM-1-positive microglia target oligodendrocytes at the border of multiple sclerosis lesions. J. Neuropathol. Exp. Neurol. 61, 539–546.
del Pilar Martin, M., Cravens, P.D., Winger, R., et al., 2008. Decrease in the numbers of dendritic cells and CD4+ T cells in cerebral perivascular spaces due to natalizumab. Arch. Neurol. 65, 1596–1603.
Waisman, A., Hauptmann, J., Regen, T., 2015. The role of IL-17 in CNS diseases. Acta Neuropathol. 129, 625–637.
Miller, D.H., Khan, O.A., Sheremata, W.A., et al., 2003. A controlled trial of natalizumab for relapsing multiple sclerosis. N. Engl. J. Med. 348, 15–23.
Johnson, K.P., 2007. Natalizumab (Tysabri) treatment for relapsing multiple sclerosis. Neurologist 13, 182–187.
Dale, A.M., Fischl, B., Sereno, M.I., 1999. Cortical surface-based analysis. I. Segmentation and surface reconstruction. NeuroImage 9, 179–194.
Fischl, B., Sereno, M.I., Dale, A.M., 1999a. Cortical surface-based analysis. II: inflation, flattening, and a surface-based coordinate system. NeuroImage 9, 195–207.
Fischl, B., Sereno, M.I., Tootell, R.B., Dale, A.M., 1999b. High-resolution intersubject averaging and a coordinate system for the cortical surface. Hum. Brain Mapp. 8, 272–284.
Chard, D.T., Jackson, J.S., Miller, D.H., Wheeler-Kingshott, C.A., 2010. Reducing the impact of white matter lesions on automated measures of brain gray and white matter volumes. J. Magn. Reson. Imaging.: JMRI 32, 223–228.
Zhang, Y., Brady, M., Smith, S., 2001. Segmentation of brain MR images through a hidden Markov random field model and the expectation-maximization algorithm. IEEE Trans. Med. Imaging 20, 45–57.
Mikolajczyk, K., Szabatin, M., Rudnicki, P., Grodzki, M., Burger, C., 1998. A JAVA environment for medical image data analysis: initial application for brain PET quantitation. Med. Inform. = Med. Et. Inform. 23, 207–214.
Turkheimer, F.E., Edison, P., Pavese, N., et al., 2007. Reference and target region modeling of [11C]-(R)-PK11195 brain studies. J. Nucl. Med.: Off. Publ. Soc. Nucl. Med. 48, 158–167.
Logan, J., Fowler, J.S., Volkow, N.D., et al., 1990. Graphical analysis of reversible radioligand binding from time-activity measurements applied to [N-11C-methyl]-(-)-cocaine PET studies in human subjects. J. Cereb. Blood Flow Metab.: Off. J. Int. Soc. Cereb. Blood Flow Metab. 10, 740–747.
Roivainen, A., Nagren, K., Hirvonen, J., et al., 2009. Whole-body distribution and metabolism of [N-methyl-11C](R)−1-(2-chlorophenyl)-N-(1-methylpropyl)−3-isoquinolinecarboxamide in humans; an imaging agent for in vivo assessment of peripheral benzodiazepine receptor activity with positron emission tomography. Eur. J. Nucl. Med. Mol. Imaging 36, 671–682.
Hammoud, D.A., Endres, C.J., Chander, A.R., et al., 2005. Imaging glial cell activation with [11C]-R-PK11195 in patients with AIDS. J. Neurovirol 11, 346–355.
Politis, M., Giannetti, P., Su, P., et al., 2012. Increased PK11195 PET binding in the cortex of patients with MS correlates with disability. Neurology 79, 523–530.
Giannetti, P., Politis, M., Su, P., et al., 2015. Increased PK11195-PET binding in normal-appearing white matter in clinically isolated syndrome. Brain: J. Neurol. 138, 110–119.
Ratchford, J.N., Endres, C.J., Hammoud, D.A., et al., 2012. Decreased microglial activation in MS patients treated with glatiramer acetate. J. Neurol. 259, 1199–1205.
Sucksdorff, M., Rissanen, E., Tuisku, J., et al., 2017. Evaluation of the effect of fingolimod treatment on microglial activation using serial PET imaging in multiple sclerosis. J. Nucl. Med.: Off. Publ. Soc. Nucl. Med.
Lockhart, A., Davis, B., Matthews, J.C., et al., 2003. The peripheral benzodiazepine receptor ligand PK11195 binds with high affinity to the acute phase reactant alpha1-acid glycoprotein: implications for the use of the ligand as a CNS inflammatory marker. Nucl. Med. Biol. 30, 199–206.
Venneti, S., Lopresti, B.J., Wiley, C.A., 2013. Molecular imaging of microglia/macrophages in the brain. Glia 61, 10–23.
Boutin, H., Murray, K., Pradillo, J., et al., 2015. 18F-GE-180: a novel TSPO radiotracer compared to 11C-R-PK11195 in a preclinical model of stroke. Eur. J. Nucl. Med. Mol. Imaging 42, 503–511.

Chauveau, F., Boutin, H., Van Camp, N., Dolle, F., Tavitian, B., 2008. Nuclear imaging of neuroinflammation: a comprehensive review of [11C]PK11195 challengers. Eur. J. Nucl. Med. Mol. Imaging 35, 2304–2319.

Marik, C., Felts, P.A., Bauer, J., Lassmann, H., Smith, K.J., 2007. Lesion genesis in a subset of patients with multiple sclerosis: a role for innate immunity? Brain: J. Neurol. 130, 2800–2815.

Sridharan, S., Lepelletier, F.X., Trigg, W., et al., 2017. Comparative Evaluation of Three TSPO PET Radiotracers in a LPS-Induced Model of Mild Neuroinflammation in Rats. Mol. Imaging Biol.: MIB: Off. Publ. Acad. Mol. Imaging 19, 77–89.

Vowinckel, E., Reutens, D., Becher, B., et al., 1997. PK11195 binding to the peripheral benzodiazepine receptor as a marker of microglia activation in multiple sclerosis and experimental autoimmune encephalomyelitis. J. Neurosci. Res. 50, 345–353.

Rovira, A., Auger, C., Alonso, J., 2013. Magnetic resonance monitoring of lesion evolution in multiple sclerosis. Ther. Adv. Neurol. Disord. 6, 298–310.

Popescu, B.F., Pirko, I., Lucchinetti, C.F., 2013. Pathology of multiple sclerosis: where do we stand? Continuum 19, 901–921.